Research Square

Preprints are preliminary reports that have not undergone peer review.
They should not be considered conclusive, used to inform clinical practice,
or referenced by the media as validated information.

Context-Specific Innate Immune Evasion via VDAC1 Gate-Jamming in Microsatellite-Stable Colorectal Cancer

Anthony J Vasquez

vasquez3921@delval.edu

Delaware Valley University https://orcid.org/0009-0000-6440-1506

Research Article

Keywords: VDAC1, gate-jamming, cGAS–STING, microsatellite-stable colorectal cancer, innate immunity, immunotherapy resistance, tGJS

Posted Date: February 26th, 2026

DOI: https://doi.org/10.21203/rs.3.rs-8935902/v1

License: This work is licensed under a Creative Commons Attribution 4.0 International License.
Read Full License

Additional Declarations: The authors declare no competing interests.

Abstract

Immune checkpoint inhibitors (ICIs) have transformed oncology for microsatellite instability-high (MSI-H) colorectal cancer, yet 85–95% of colorectal cancer patients carry microsatellite-stable (MSS) tumors and derive no benefit from current ICI regimens. We propose that VDAC1-mediated mitochondrial DNA (mtDNA) gate-jamming — suppression of VDAC1 oligomerization by HK-II docking, Bcl-xL binding, and outer mitochondrial membrane cholesterol loading — explains this selectivity by silencing the cGAS–STING innate immune signal required for spontaneous T cell priming. To test this hypothesis at scale, we computed a transcriptomic Gate-Jamming Score (tGJS = 0.4 × HK2 + 0.3 × BCL2L1 + 0.3 × TSPO, rank-normalized) and conducted three sequential analyses: (S1) pan-cancer TCGA (n = 10,071, 33 cancer types) — null result (ρ = +0.38 vs ICI response rate, p = 0.14); (S2) COADREAD MSS/TP53-wildtype clean room (n = 209) — five Bonferroni-significant inverse correlations between tGJS and immune markers including HAVCR2 (ρ = −0.349, p_bonf = 5×10^{-6}), CXCL10 (ρ = −0.231, p_bonf = 0.015), and cGAS (ρ = −0.208, p_bonf = 0.049); (S3) IMvigor210 urothelial carcinoma atezolizumab cohort (n = 348) — null result (Wilcoxon p = 0.965, Cox HR = 0.898, p = 0.455). The flanking nulls (S1, S3) define the framework's domain: the gate-jamming signal is detectable only when VDAC1-mediated mtDNA release is the dominant cytosolic DNA source and innate priming is the rate-limiting step. The S2 clean room results, combined with the three-layer therapeutic hypothesis (VDAC1 gate-opener + cGAMP/DNA eraser inhibitor + checkpoint blockade) independently derived from the same data by three AI analytical systems, motivates protein-level validation in MSS colorectal cancer and combination ICI trials in this specific population.

1. Introduction

Colorectal cancer is the second leading cause of cancer mortality in the United States, with approximately 150,000 new cases annually. Pembrolizumab and nivolumab achieve durable responses in the ~ 5–15% of patients with MSI-H tumors — where pervasive genomic instability generates abundant mutational neoantigens and activates innate immune sensing. For the remaining 85–95% of patients with MSS tumors, ICI monotherapy has consistently failed in randomized trials, and no predictive biomarker identifies a responsive MSS subpopulation. The central unmet need in colorectal cancer immunotherapy is converting MSS tumors from immune-cold to immune-hot.

VDAC1 (voltage-dependent anion channel 1) is the most abundant protein in the outer mitochondrial membrane, present at densities exceeding 1,000 molecules per μm². Its oligomeric form releases 500–650 bp mitochondrial DNA (mtDNA) fragments into the cytoplasm (Kim et al. 2019, Science), activating the cGAS–STING innate immune pathway required for spontaneous CD8 + T cell priming (Woo et al. 2014, Immunity). Cancer cells suppress this oligomerization through at least three mechanisms: hexokinase-II (HK-II) docking on VDAC1's outer barrel (Wolf et al. 2023, Science Immunology; Bieker et al. 2025, Communications Biology), Bcl-xL binding via its BH4 domain (Monaco et al. 2015, JBC), and cholesterol loading of the outer mitochondrial membrane (Betaneli et al. 2012, Biophysical Journal).

Together, these constitute a gate-jamming architecture that silences the mitochondrial innate immune alarm.

Critically, this mechanism is predicted to be relevant precisely in MSS tumors. In MSI-H tumors, nuclear DNA damage generates cytosolic DNA fragments independently of mitochondrial dynamics, saturating cGAS–STING regardless of VDAC1 state. In MSS tumors where nuclear DNA damage is minimal, VDAC1-mediated mtDNA release is the predicted dominant — potentially sole — cytosolic DNA source. Gate-jamming in this context suppresses the entire innate priming axis, explaining ICI failure without invoking T cell exhaustion.

We formalized this hypothesis as a transcriptomic Gate-Jamming Score (tGJS) and conducted three sequential analyses designed to test the framework, define its domain, and identify the biological context where protein-level validation is most warranted.

2. Methods

2.1 Transcriptomic Gate-Jamming Score

The tGJS is a rank-normalized composite of three genes encoding the primary VDAC1 gate-jamming proteins:

tGJS = 0.40 × norm(HK2) + 0.30 × norm(BCL2L1) + 0.30 × norm(TSPO)

HK2 encodes hexokinase-II (VDAC1 docking, weight 0.40); BCL2L1 encodes Bcl-xL (VDAC1 binding, weight 0.30); TSPO encodes the Translocator Protein, a cholesterol transport protein used as a proxy for mitochondrial cholesterol loading (weight 0.30). Normalization is performed within each cohort.

2.2 S1: Pan-Cancer TCGA Analysis

Expression data for 10,071 samples across 33 TCGA cancer types were retrieved from the TCGA PanCanAtlas (cBioPortal, pan_cancer_atlas_2018). ICI response rates per cancer type were compiled from published meta-analyses. tGJS was correlated with per-cancer-type mean ICI response rate using Spearman rank correlation.

2.3 S2: COADREAD MSS-Stratified Clean Room Analysis

592 COADREAD samples from coadread_tcga_pan_can_atlas_2018 were stratified by MSI status × TP53 mutation into four groups. MSI status was determined from MANTIS (threshold ≥ 0.4) and MSISensor (threshold > 10) scores; MSI-H if either score exceeded threshold. TP53 mutation status was retrieved from the COADREAD mutation profile. Spearman correlations were computed between tGJS and 20 immune/pathway markers in each stratum, with Bonferroni correction for 20 comparisons per stratum.

2.4 S3: IMvigor210 Atezolizumab Cohort

The IMvigor210CoreBiologies R package (Mariathasan et al. 2018) provides pre-treatment bulk RNA-Seq from 348 urothelial carcinoma patients treated with atezolizumab, with RECIST response, overall survival, TMB, IC Level, and immune phenotype classification. Raw counts were converted to TPM. tGJS was computed using z-score normalization within the cohort. Primary tests: Wilcoxon rank-sum, logistic regression, Spearman ρ vs ordinal RECIST, Cox proportional hazards, and log-rank (tGJS high vs low).

2.5 Multi-Model Convergence Protocol

The gate-jamming therapeutic hypothesis was evaluated using the IRIS (Independent Replicated Inquiry System) protocol, in which five independent large language models (Claude Opus 4.6, Gemini 2.5 Pro, Grok 4.1 Fast, Mistral Large, DeepSeek Chat) received the identical compiled question without cross-exposure. Claims were extracted and embedded using all-MiniLM-L6-v2 (384-dimensional), clustered by cosine similarity ≥ 0.70, and classified by model agreement (TYPE 0 = 4–5 models, TYPE 1 = 3/5, TYPE 2 = 2/5, TYPE 3 = 1/5). Cross-run analysis across 28 independent runs (27,931 pairwise comparisons) assessed inter-run replication

3. Results

3.1 S1: Pan-Cancer tGJS Does Not Predict ICI Response (n = 10,071)

Across 33 TCGA cancer types, tGJS was not inversely correlated with published ICI response rates (Spearman ρ = +0.382, p = 0.144). The positive trend reflects that metabolically aggressive tumors — which have higher tGJS — tend to be the same tumors with higher mutational burden and baseline immune activation, creating a confound that overwhelms any gate-jamming signal at the cross-cancer level. ENPP1 expression showed the strongest pan-cancer inverse correlation with tGJS ($\rho = -0.181$, $p = 4.3 \times 10^{-75}$), initially interpreted as evidence of orthogonal evasion strategies. The pan-cancer null is consistent with the hypothesis that a cancer-type-homogeneous, immunogenomically stratified analysis is required to observe the gate-jamming signal. Full results are in Supplementary Analysis S1.

3.2 S2: MSS/TP53-wt Clean Room Recovers Five Bonferroni-Significant Signals (n = 209)

Restricting analysis to the MSS/TP53-wildtype COADREAD stratum recovered five markers reaching Bonferroni significance (Table 1), all in directions predicted by the gate-jamming hypothesis.

Table 1

Bonferroni-significant correlations in the MSS/TP53-wt clean room (n = 209).

Marker	Spearman ρ	p_bonf	Direction	Interpretation
HAVCR2 (TIM-3)	−0.349	5×10^{-6}	Down	Fewer T cells infiltrate to become exhausted
TREX1	+ 0.315	7×10^{-5}	Up	Co-deployment of mtDNA erasure with gate-jamming
CXCL10	−0.231	0.015	Down	Reduced IFN-γ–induced chemokine recruitment
STING ratio	−0.216	0.034	Down	Residual STING signaling shifts to immunosuppressive profile
cGAS (MB21D1)	−0.208	0.049	Down	Lower cGAS in high-tGJS tumors

No immune markers reached Bonferroni significance in the MSI-H control strata (n = 67 and n = 28), consistent with the prediction that genomic instability saturates cGAS–STING independently of VDAC1 state.

The ENPP1 anti-correlation (ρ = −0.027, not significant) did not replicate within the clean room, correcting the S1 interpretation: the pan-cancer ENPP1 signal was driven by cross-cancer-type expression differences rather than a within-tumor-type biological relationship.

Two unexpected findings refined the evasion architecture model. First, the positive correlation between tGJS and TREX1 (ρ = +0.315) indicates that the most evasion-committed MSS tumors co-deploy mitochondrial gate-jamming and cytosolic DNA erasure simultaneously — a belt-and-suspenders strategy rather than an either/or trade-off. Second, HAVCR2 (TIM-3) showed the strongest anti-correlation, suggesting high-tGJS MSS tumors suffer from T cell absence rather than T cell exhaustion — consistent with suppressed innate priming preventing initial T cell recruitment. Full stratified results across all 20 markers and 4 strata are in Supplementary Analysis S2.

3.3 S3: tGJS Does Not Predict Atezolizumab Response in Urothelial Carcinoma (n = 348)

In the IMvigor210 cohort, tGJS showed no association with atezolizumab response or overall survival at any level of analysis (Table 2).

Table 2
IMvigor210 primary results (n = 348, n_response = 298).

Test	Result	p-value
Wilcoxon (CR/PR vs SD/PD)	—	0.965
Logistic regression	OR = 1.038	0.868
Spearman ρ vs RECIST	ρ = −0.017	0.767
Kruskal–Wallis by tertile	—	0.559
Cox PH (continuous)	HR = 0.898 (95% CI: 0.678–1.190)	0.455
Log-rank (high vs low)	—	0.587
Median OS, tGJS-High	20.6 months	—
Median OS, tGJS-Low	20.6 months	—

This null is mechanistically expected: urothelial carcinoma carries high baseline somatic mutation burden from tobacco and occupational carcinogen exposure, generating nuclear DNA-derived cytosolic DNA independently of VDAC1 state. Additionally, atezolizumab targets the adaptive immune checkpoint on exhausted T cells downstream of innate priming; even if gate-jamming were relevant, its effect would operate upstream of the treatment's mechanism of action. Full results and four figures are in Supplementary Analysis S3.

4. Discussion

4.1 Three Analyses Define the Framework's Domain

The S1 → S2 → S3 arc is the central finding of this work. It answers not only 'is there a signal?' but 'where does the signal live?':

Table 3
Three-cohort analysis arc.

Analysis	Cohort	Context	tGJS Signal
S1	TCGA pan-cancer (n = 10,071)	33 cancer types, ICI response proxy	Null — cross-cancer confounds
S2	TCGA COADREAD MSS/TP53-wt (n = 209)	Clean room: MSS + intact apoptosis	5 Bonferroni-significant immune correlations
S3	IMvigor210 urothelial (n = 348)	High TMB, PD-L1 blockade	Null — wrong context, wrong treatment mechanism

The two nulls are not failures — they are the framework's falsification boundaries. A signal that appears everywhere is not a mechanism; it is noise. A signal that appears precisely where the biology predicts it

should appear, and not where the biology predicts it shouldn't, is evidence that the model is capturing something real. The COADREAD MSS/TP53-wildtype stratum represents the tightest available approximation of the predicted clean room using existing public data: minimal nuclear DNA instability, intact TP53 apoptosis signaling, VDAC1 as the predicted dominant cytosolic DNA source.

4.2 The Therapeutic Hypothesis: Three Independent Systems, One Stack

The analytical arc motivates a specific three-layer therapeutic intervention. This hypothesis was independently derived by three AI analytical systems (Claude Opus, Gemini Pro, Grok) working from the same data without cross-exposure, converging on identical components:

1. **VDAC1 gate-opener:** displace HK-II from VDAC1 (methyl jasmonate, 2-DG, clotrimazole) to restore oligomerization-dependent mtDNA release and cGAS–STING activation.
2. **DNA/cGAMP eraser inhibitor:** inhibit TREX1 or ENPP1 to prevent degradation of the released mtDNA or downstream cGAMP, amplifying and sustaining innate immune activation.
3. **Checkpoint blockade:** administer anti-PD-1/PD-L1 to prevent exhaustion of T cells now being recruited by the restored innate signal.
   The order matters: gate-opener generates the innate signal; eraser inhibitor sustains it; checkpoint blockade amplifies the adaptive response. The TREX1 co-occurrence finding from S2 directly informs step two: high-gate-jamming tumors simultaneously upregulate cytosolic DNA erasure, implying gate-opener alone may be insufficient. Three independently reasoning systems arriving at the same three-layer stack from the same data constitutes a prior strong enough to justify the next experiment.

4.3 Why MSS Colorectal Is the Right Target

MSS colorectal adenocarcinoma has: (1) the largest absolute population of ICI-refractory patients among common cancers where ICI is attempted; (2) well-characterized MSI stratification, allowing clean separation of the signal; (3) an available TP53 mutation axis that further refines the predicted clean room; and (4) a tumor biology where VDAC1 docking by HK-II is supported by multiple independent lines of evidence. The HAVCR2 finding ($\rho = -0.349$) points to T cell absence rather than T cell exhaustion as the immune bottleneck in high-tGJS MSS tumors — a meaningful clinical distinction suggesting anti-TIM-3 trials in MSS CRC are addressing the wrong checkpoint.

4.4 The GJS as One Layer of a Multi-Layer Evasion Architecture

The GJS measures one specific bottleneck — VDAC1 oligomerization suppression — within a multi-layer immune evasion system. The cGAS–STING axis is not uniformly anti-tumor: Lai et al. (2025, Immunity) showed that VDAC-mediated mtDNA from senescent tumor cells can enhance immunosuppression through MDSC recruitment. The tumor microenvironment may override gate-restoration even when

cGAS–STING is successfully activated. STING pathway competence must be assessed — STING silencing via promoter methylation occurs in 1–25% of tumors pan-cancer, and high-GJS tumors with silenced STING require epigenetic reactivation before gate-restoration can be effective.

Table 4
GJS × STING status therapeutic matrix.

	STING Intact	STING Silenced
High GJS	Primary target — gate-opener + eraser inhibitor + checkpoint	Requires DNMT inhibitor before gate-restoration
Low GJS	Gate open, pathway active — checkpoint alone may suffice	Chronic signaling, paradoxical immunosuppression

4.5 What the tGJS Does Not Capture

The transcriptomic proxy measures mRNA abundance of three genes; it cannot distinguish HK-II docked on VDAC1 versus in the cytosol, Bcl-xL bound to VDAC1 versus other targets, or TSPO-mediated cholesterol at the outer mitochondrial membrane versus elsewhere. Protein-level measurement — proximity ligation assay for HK-II–VDAC1 and Bcl-xL–VDAC1 complexes, mitochondrial lipidomics for the Chol/CL ratio — is required to compute the true GJS:

GJS = f_HKII × 0.40 + f_BclxL × 0.30 + [Chol]/[CL]_norm × 0.30
where f_HKII is the fraction of VDAC1 occupied by HK-II and f_BclxL the fraction bound by Bcl-xL (both 0–1). The tGJS is a screening tool to identify where this protein-level assay should be run first.

4.6 Limitations

4. **No experimental validation.** All findings are computational. The weights (0.4/0.3/0.3) are convergence-derived estimates, not empirically optimized coefficients.
5. **Bulk RNA-Seq.** Expression values are cellular averages across tumor, stromal, and immune cells. Single-cell attribution is required to determine which cell type drives the tGJS signal.
6. **TCGA lacks treatment data.** The S2 correlations are with immune markers, not ICI outcomes. The hypothesis that high-tGJS MSS CRC tumors fail ICI is mechanistically motivated but not directly tested.
7. **IMvigor210 is a single cohort.** The S3 null applies to urothelial carcinoma treated with PD-L1 blockade. It does not predict the outcome in MSS CRC treated with combination gate-restoration regimens.
8. **VBIT-4 specificity.** Ravishankar et al. (2025, bioRxiv) showed VBIT-4 disrupts membranes independent of VDAC1 at ≥ 30 μM. Claims requiring VBIT-4 need orthogonal genetic validation.
9. **TREX1 inhibitors are not clinically available.** This identifies a drug development gap.

4.7 Immediate Next Steps

- **In vitro (4–8 weeks)**: Displace HK-II from VDAC1 in immune-cold cell lines (Panc-1, HCT116) and measure cytoplasmic mtDNA, p-STING (Ser366), and IFN-β. Compute GJS across 15 + cell lines and correlate with basal cGAS–STING activity (Spearman ρ ≤ −0.6 predicted).
- **Protein-level validation in COADREAD tissue (8–12 weeks)**: Run proximity ligation assay for HK-II–VDAC1 complexes in MSS vs MSI-H colorectal cancer tissue sections. Correlate PLA signal with CD8A IHC and tGJS.
- **In vivo (10 weeks)**: Gate-restoration combination (methyl jasmonate + ABT-263) + anti-PD-1 in 4T1 (immune-cold) and MC38 (immune-hot) syngeneic tumor models. Prediction: synergy in 4T1, no added benefit in MC38.
- **GSE91061 melanoma validation**: The Riaz 2017 nivolumab cohort (n = 109) is the next planned validation to confirm the boundary conditions in a second high-TMB tumor type.

5. Data Availability

- **Analysis scripts**: analysis/tcga_gjs/compute_tgjs.py, compute_tgjs_coadread_mss.py; analysis/imvigor210/compute_tgjs_imvigor210.R
- **Repository**: github.com/templetwo/vdac-pharmacology-atlas
- **Dataset archive**: huggingface.co/datasets/TheTempleofTwo/vdac-pharmacology-atlas
- **OSF preregistration**: osf.io/c9rqb/
- **IRIS Gate Evo pipeline**: github.com/templetwo/iris-gate-evo

Declarations

Data Availability

- **Analysis scripts:** analysis/tcga_gjs/compute_tgjs.py, compute_tgjs_coadread_mss.py; analysis/imvigor210/compute_tgjs_imvigor210.R
- **Repository:** github.com/templetwo/vdac-pharmacology-atlas
- **Dataset archive:** huggingface.co/datasets/TheTempleofTwo/vdac-pharmacology-atlas
- **OSF preregistration:** osf.io/c9rqb/
- **IRIS Gate Evo pipeline:** github.com/templetwo/iris-gate-evo

Author Contributions

A.J.V. conceived the research questions, designed the analytical framework, executed all computational analyses, interpreted all results, and wrote the manuscript. Computational analyses were executed with Claude Code (Anthropic). Manuscript drafting was assisted by Claude (Anthropic). The IRIS multi-model

convergence protocol was developed and run by A.J.V. using five independent AI systems (Claude Opus, Gemini Pro, Grok, Mistral, DeepSeek); convergence metrics are system-computed. All scientific decisions, interpretations, and conclusions are solely the responsibility of A.J.V.

Competing Interests

The author declares no competing interests. This work received no external funding.

License

This manuscript and all associated data are released under CC BY 4.0.

References

1. Betaneli V, Petrov EP, Schwille P. (2012) The role of lipids in VDAC oligomerization. Biophys J 102:523.
2. Bieker JT, Timme S, et al. (2025) A membrane-buried glutamate mediates VDAC–hexokinase binding. Commun Biol 8:212.
3. Carozza JA, et al. (2023) ENPP1 as an innate immune checkpoint. PNAS.
4. Daniilidis M, Gunsel U, et al. (2025) Structural basis of apoptosis induction by VDAC1. Nat Commun 16:9481.
5. Fadzeyeva E, et al. (2026) CBD-induced VDAC1 oligomerization-dependent effects. Pharmaceuticals 19:95.
6. Gehrcken L, et al. (2025) cGAS–STING in anti-tumor immunity. Adv Sci 12:2500296.
7. Goicoechea L, et al. (2023) Mitochondrial cholesterol: metabolism and impact on redox biology. Redox Biol 61:102643.
8. Ikeda H, et al. (2025) Mitochondrial transfer from cancer cells to TILs. Nature.
9. Jahn H, Bartos L, Dearden GD, et al. (2023) VDAC1 dimers as phospholipid scramblases. Nat Commun 14:8115.
10. Kim J, et al. (2019) VDAC oligomers form mitochondrial pores to release mtDNA. Science 366:1531.
11. Lafargue K, et al. (2025) Lipid regulation of VDAC1 assemblies. Commun Biol 8:936.
12. Lai J, et al. (2025) VDAC-mediated mtDNA release from senescent tumor cells. Immunity 58:811.
13. Mangalhara KC, et al. (2023) Complex II loss activates MHC-I. Science 381:1316.
14. Mariathasan S, et al. (2018) TGFβ attenuates tumour response to PD-L1 blockade by contributing to exclusion of T cells. Nature 554:544.
15. Monaco G, et al. (2015) The BH4 domain of Bcl-xL targets VDAC1 for Ca^{2+} control. J Biol Chem 290:9150.

16. Montero J, et al. (2008) Mitochondrial cholesterol contributes to chemotherapy resistance in HCC. Cancer Res 68:5246.
17. Prashar A, et al. (2024) VDAC1-dependent inner membrane herniation vesicles. Nature 632:1110.
18. Ravishankar H, et al. (2025) VBIT-4 specificity challenge. bioRxiv.
19. Ren H, et al. (2025) VSTM2L enhances HK2–VDAC1 interaction. Nat Commun 16:1534.
20. Rimmerman N, et al. (2013) Direct modulation of the OMM channel VDAC1 by CBD. Cell Death Dis 4:e949.
21. Samson N, Ablasser A. (2022) The cGAS–STING pathway and cancer. Nat Cancer 3:1452.
22. Shoshan-Barmatz V, et al. (2025) p53 directly binds VDAC1. Biomolecules 16:141.
23. Wan X, et al. (2026) VDAC1 oligomerization regulates PANoptosis. Neural Regen Res 21(4).
24. Wolf AJ, et al. (2023) HK2 dissociation from VDAC1 triggers NLRP3. Sci Immunol 8:eade7652.
25. Woo SR, et al. (2014) STING-dependent cytosolic DNA sensing mediates innate immune recognition of tumors. Immunity 41:830.
26. Xian H, et al. (2022) Oxidized mtDNA exit via mPTP and VDAC channels. Immunity 55:1370.

Figures

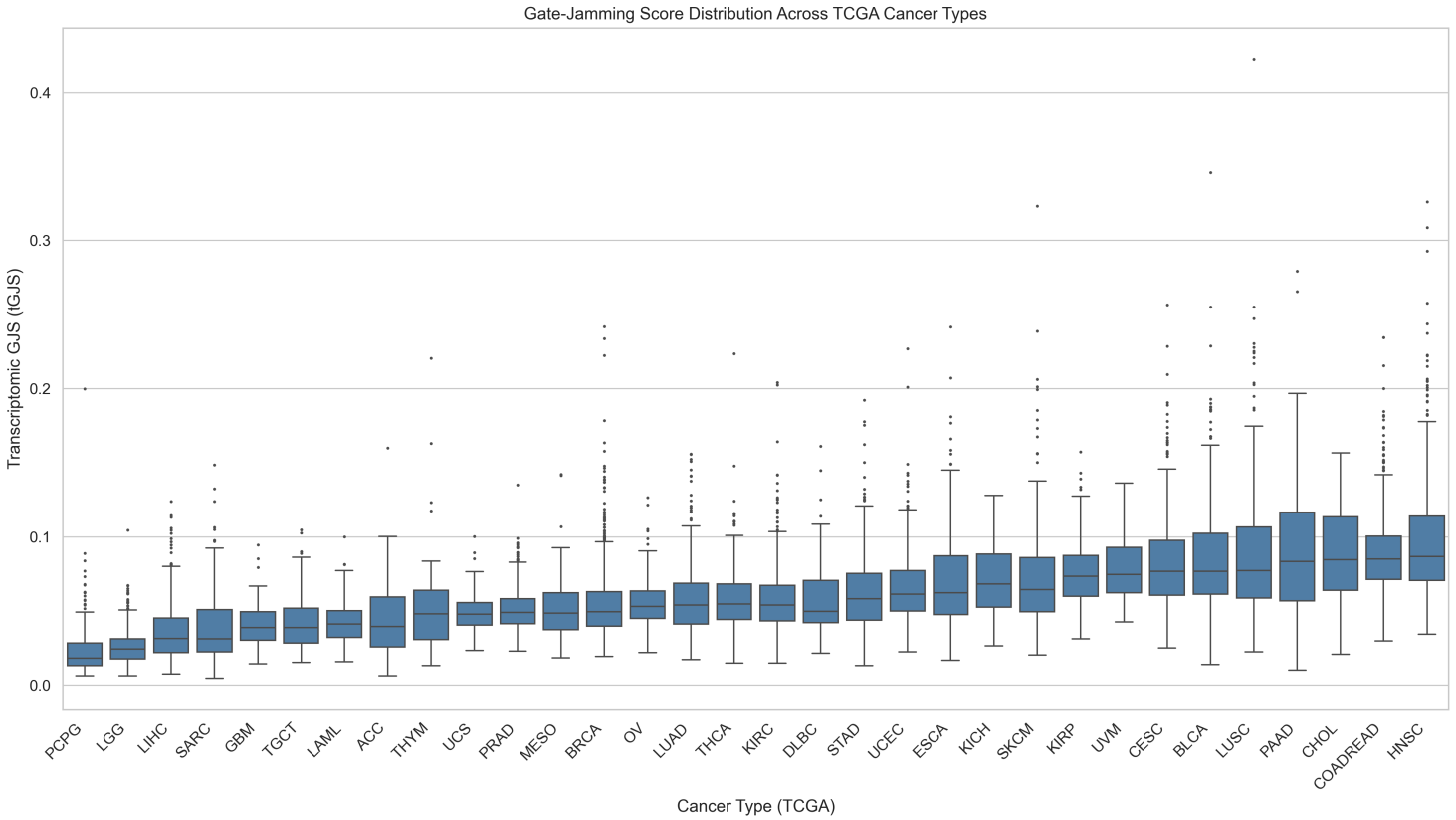


Figure 1

Legend not included with this version.

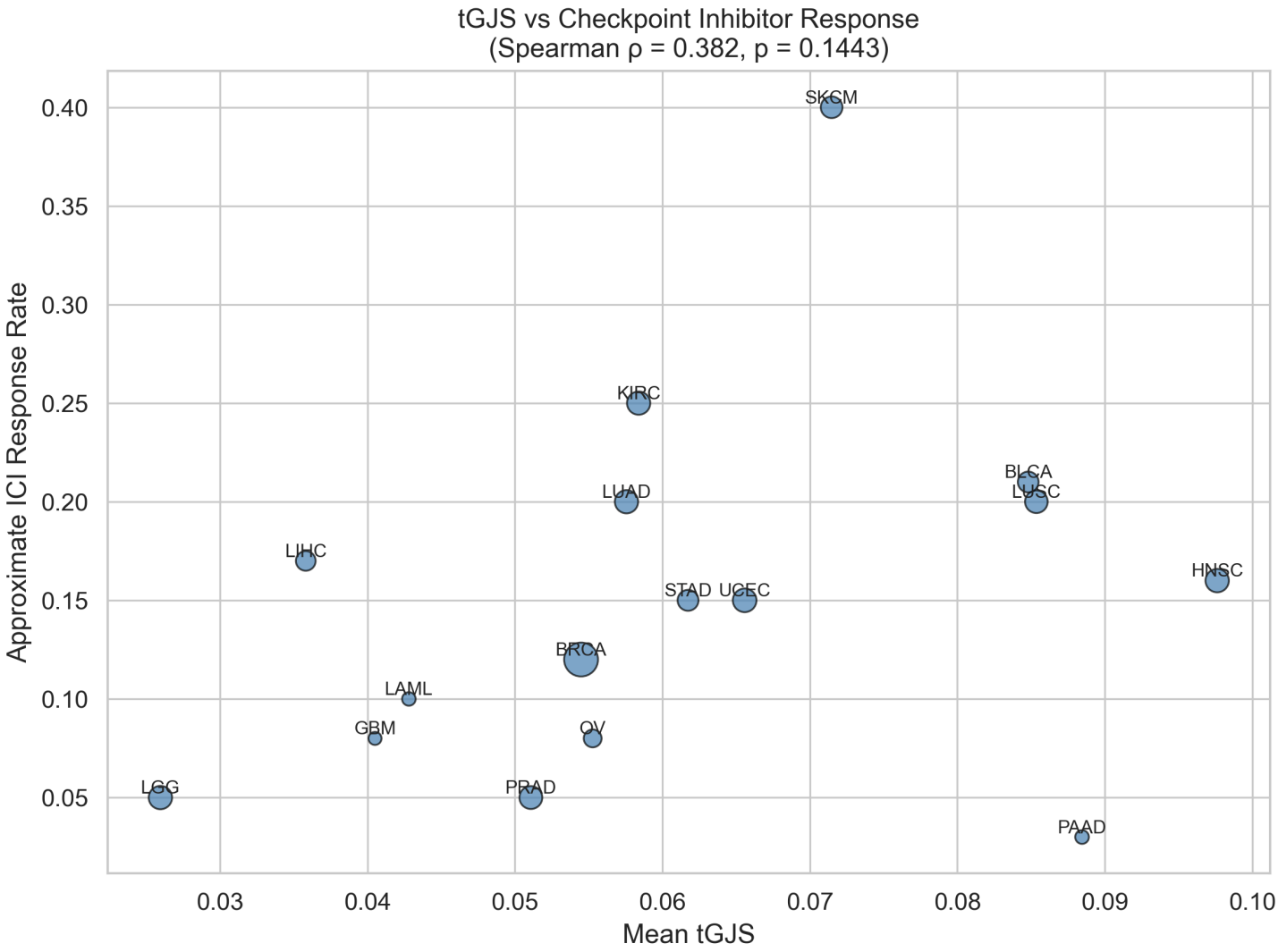


Figure 2

Legend not included with this version.

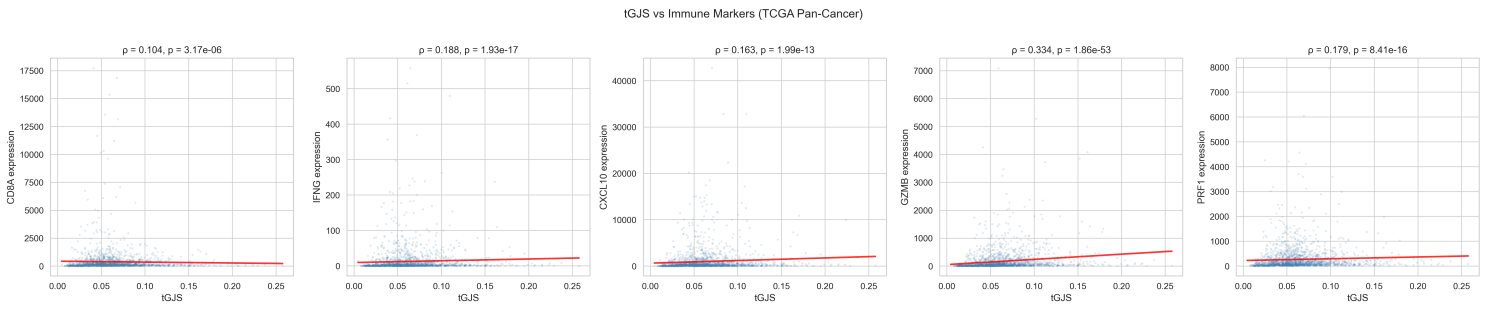


Figure 3

Legend not included with this version.

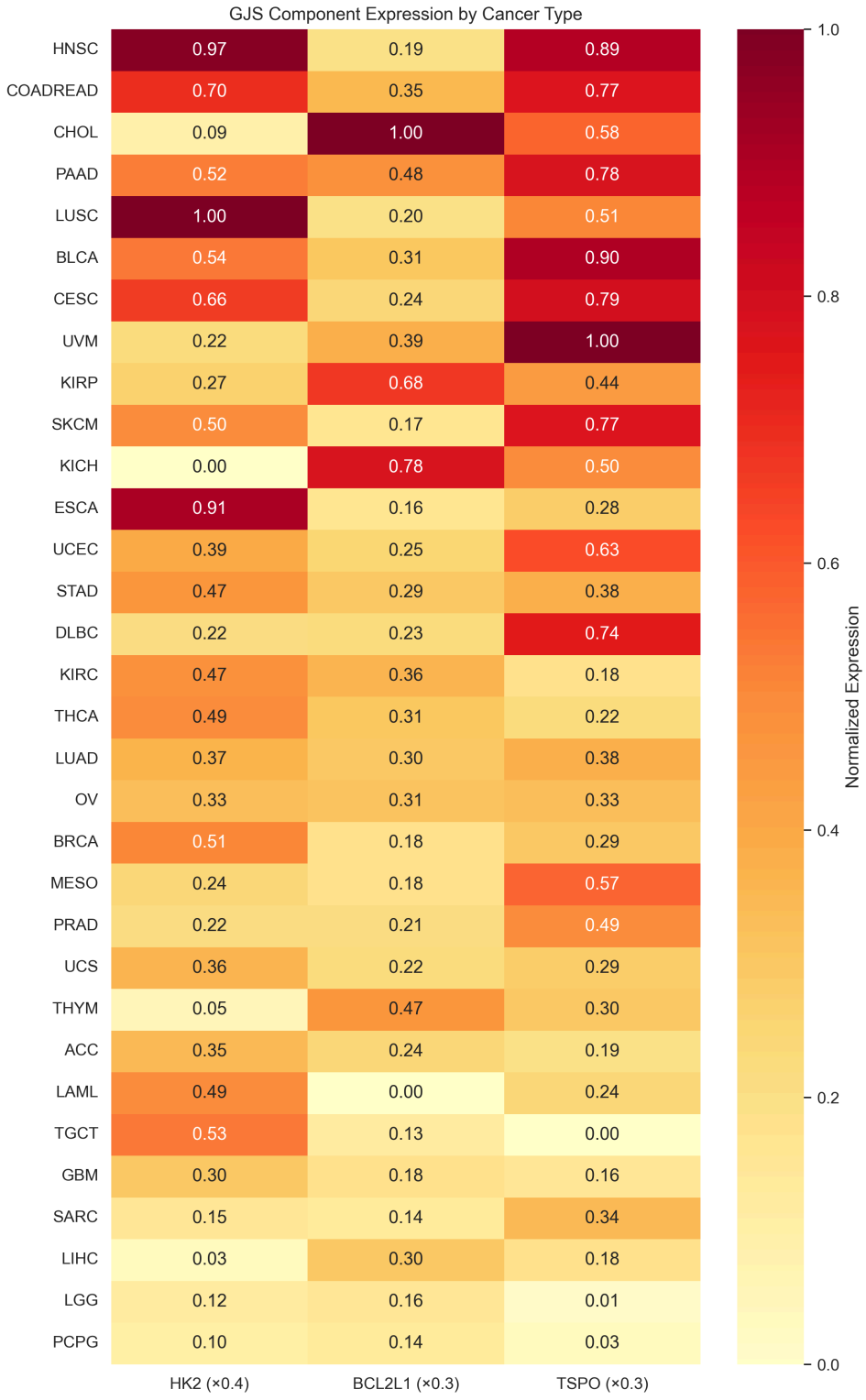


Figure 4

Legend not included with this version.

Supplementary Files

This is a list of supplementary files associated with this preprint. Click to download.

- supplementaryS1tcgaboundaryanalysis.docx
- supplementaryS2coadreadmss.docx
- supplementaryS3imvigor210.docx
- figS3atgjsbyrecist.png
- figS3bresponseratebytertile.png
- figS3ctgjstmbinteraction.png
- figS3dkmosbytgjs.png